Israel Journal of Ecology & Evolution, 2016
Vol. 61, No. 2, 95–105, http://dx.doi.org/10.1080/15659801.2015.1124656

Taylor & Francis
Taylor & Francis Group

Coordination of sniffing and whisking depends on the mode of interaction with the environment

Ehud Fonio[a]*, Goren Gordon[b], Noy Barak[c], Yonatan Winetraub[d], Tess Baker Oram[c], Sebastian Haidarliu[c], Tali Kimchi[c] and Ehud Ahissar[c]

[a]*Department of Physics of Complex Systems, Weizmann Institute of Science, Rehovot, Israel;* [b]*Department of Industrial Engineering, Tel-Aviv University, Tel-Aviv, Israel;* [c]*Department of Neurobiology, Weizmann Institute of Science, Rehovot, Israel;* [d]*Department of Structural Biology, Stanford University, Stanford, CA, USA*

(*Received 30 October 2014; accepted 22 November 2015*)

Smell and touch convey most of the information that nocturnal rodents collect in their natural environments, each via its own complex network of muscles, receptors and neurons. Being active senses, a critical factor determining the integration of their sensations relates to the degree of their coordination. While it has been known for nearly 50 years that sniffing and whisking can be coordinated, the dynamics of such coordination and its dependency on behavioral and environmental conditions are not yet understood. Here we introduce a novel non-invasive method to track sniffing along with whisking and locomotion using high-resolution video recordings of mice, during free exploration of an open arena. Active sensing parameters in each modality showed significant dependency on exploratory modes ("Outbound", "Exploration" and "Inbound") and locomotion speed. Surprisingly, the correlation between sniffing and whisking was often as high as the bilateral inter-whisker correlation. Both inter-whisker and inter-modal coordination switched between distinct high-correlation and low-correlation states. The fraction of time with high-correlation states was higher in the Outbound and Exploration modes compared with the Inbound mode. Overall, these data indicate that sniffing–whisking coordination is a complex dynamic process, likely to be controlled by multiple-level inter-modal coordinated loops of motor-sensory networks.

Keywords: active sensing; sniffing and whisking behavior; bi-modal sensation; motor-sensory coordination; non-invasive tracking; freely moving mice

Introduction

Nocturnal rodents, such as rats and mice, actively acquire information from their surroundings via behaviors known as whisking (Vincent 1912; Gao et al. 2001; Berg & Kleinfeld 2003; Knutsen et al. 2006; Mitchinson et al. 2007; Grant et al. 2009; Zuo et al. 2011) and exploratory sniffing (Macrides et al. 1982; Uchida & Mainen 2003; Kepecs et al. 2007; Wesson et al. 2008). Touch and smell are two of the most prominent senses of these animals and are being used extensively in their everyday life. In contrast to the wealth of studies addressing each of these modalities separately for almost a century, there have been only a handful of studies addressing their interactions (reviewed in Deschênes et al. 2012), of which only one was performed on freely ranging animals (Ranade et al. 2013) and none were in a non-invasive way. In a seminal paper, Welker described a mode of correlated sniffing and whisking movements in rats when their noses touched objects (Welker 1964). Relations between whisking and sniffing have been further discussed during theta-synchronized sniffing behaviors (Semba & Komisaruk 1984) and during odor discrimination (Kepecs et al. 2007). Recently, it was shown that at least some of the phases of whisking and sniffing are controlled by the same central pattern generator (Moore et al. 2013), and that these two movements are often correlated during palpations (Cao et al. 2012).

The aforementioned studies examined sensory behavior in an unnatural context where the animal was head fixed. While this approach is useful for studying well-defined components of neural processing, often behaviors observed in such semi-artificial conditions are not relevant to the animal's *umwelt* (i.e. the world from the perspective of the animal's point of view; Uexküll 1957). Adopting a complementary ethological approach, where the animal is being observed in a natural-like context, is important in order to get more relevant and comprehensive description of the richness, variability and complexity of innate behavior. Such a broader perspective increases the chances that the measured behavior represents meaningful processes. As previously shown when mice are given the opportunity to freely explore a new terrain, they iteratively enter into the external area for a short while, then return to the home-cage, showing a gradual build-up of explorative degrees of freedom where successive entries become more complex and less predictive (Fonio et al. 2009). This behavioral structure was described in the more general context of the home-base behavior (Eilam & Golani 1989) and excursions from the home-base which are a natural building block of exploratory behavior (Golani et al. 1993; Tchernichovski et al. 1998; Gordon et al. 2014). However, most behavioral studies of this sort

*Corresponding author. Email: ehud.fonio@weizmann.ac.il

have been restricted to one modality (e.g. vision, touch, smell, but see, for example, Koelewijn et al. 2010 and Gordon et al. 2014). Studying the complex agent-environment system and analyzing multi-modal motor-sensory behavior in natural-like conditions is thus a desirable, though a challenging step.

Here, we utilized the ethological approach of free exploration, using the natural segmentation of the behavior into reiterated round-trips from the home-nest into the external surroundings (Fonio et al. 2009) and combine a natural-like apparatus, where mice and their growing pups were allowed to freely move between their secure home-nest and an exposed arena, with a high-resolution tracking of bi-modal active sensing behavior of whisking and sniffing. We begin this report by describing a new method for a non-invasive, video-based sniffing tracking along with its anatomical basis and empirical validation. We then show that the repeated round-trips to the exposed arena are composed of three distinct exploratory modes, and present kinematic and spectral analysis of the behavior with respect to the two modalities – sniffing and whisking – and head and body motion. We show that sniffing and whisking are usually coordinated during exploratory active sensing, in which animals maintain correlated active sensing, and that their coordination depends on the exploratory mode.

Material and methods

Animals and behavioral apparatus

A family of C57BL/6 mice (a mature female and her three pups) was raised in a "natural habitat" apparatus in which the animals were allowed to freely traverse between a secure shelter (nest-cage) and a novel environment. The female and newborn pups (P4) were housed in the special nest-cage made from Perspex that was partitioned into two compartments (Figure 1(a), Section 1 in the Supplemental data). The first compartment (marked in yellow) contained wood-chips and standard dry food pallets that were given *ad libitum* and in the second compartment (marked in orange) there was free access to water. A shallow angle ramp (30 deg.) connected the two compartments. During the first weeks, the pups huddled in the first compartment until reaching the age of P21–23 when they began to move around the nest-cage. At that time, a small door (3 cm × 3 cm) in the second compartment (marked in red), leading to a novel area, was opened, thus allowing free passage between the nest-cage and that area, both for the pups and their mother. The behavior during round-trips into the novel area was recorded using a high-speed video camera (Optronis CL600×2) at 500 frames/sec, 1280 × 1024 pixels. The setup was designed to allow constant high-resolution video recording for several hours.

The behavior was recorded at night, which is the active phase of these nocturnal rodents, and in a dark room. A 9″ × 9″ IR illuminator (Metaphase) was placed under the transparent floor of the novel area and was used as a uniform backlight illumination for the camera. Animal maintenance and all experimental procedures were conducted in accordance with National Institutes of Health and The Weizmann Institute of Science guidelines (IACUC approval # 01400310-2).

Data acquisition

Data acquisition was initiated once the pups approached to the door for the first time which occurred at P21 (i.e. 21 days postnatal). The data were acquired during 3 nights at ages P21, P23 and P27. We collected in total of 304 movies of variable durations (see, for example, Video S1), summing up to 843,401 tracked frames (1700 sec) of the mouse behavior while they were performing round-trips outside the nest-cage. These videos were tracked by the BIOTACT Whisker Tracking Tool (BIOTACT consortium; Perkon et al. 2011), giving for each frame relevant information about head position, snout contour, the position of the tip of the nose and orientation of whiskers on both sides of the snout (Figure 1(b), Video S2). In each video, some frames were not tracked properly, either due to vertical movements of the snout or touching of the whiskers with objects in the novel area. These frames were discarded by using the head contour goodness-of-fit parameter (Figure 1(d)) that is automatically calculated by the tracker (Perkon et al. 2011). This reduced the number of analyzed frames to 515,318 frames (126,134 in the Outbound mode, 308,528 in the Exploration mode and 80,656 in the Inbound mode). Furthermore, in order to calculate the head velocity, the head trajectory was smoothed by a moving average of size 100 msec (50 frames).

Acquisition of sniffing behavior

Based on the coordinates of the snout contour and the tip of the nose, both of which are given as output by the BIOTACT Whisker Tracker described above, a non-invasive image-processing-based sniffing detection algorithm was developed and implemented in Mathematica® (Wolfram) and Matlab® (MathWorks). For each frame (Figure 1(b)), the automatic tracking tool extracted the coordinates of the snout contour and the nose tip (Perkon et al. 2011). The snout contour (Figure 1(b) in red) was then smoothed with a moving window of size 10 msec (5 frames) and centered on the nose tip. For each point in the smoothed contour, the angle between it and the two adjacent points was calculated, $\alpha(s)$, where s is the arc length along the snout contour. The angle's spatial derivative was then calculated $\partial_s\alpha(s) = d\alpha(s)/ds$ and smoothed with a moving window of 0.75 mm (Figure 1(c) in red). The points of contour curvature were found as those in which the angle's derivative changed signs, $c_n = \left(s \mid \partial_s\alpha(s-1)\times\partial_s\alpha(s+1) < 0\right)$, for $n = -N, \ldots, -1, 1, \ldots, N$, where negative n are to the left to the nose tip and positive n are right to the nose tip, i.e. c_{-1}, c_{+1} are the two contour curvature points adjacent to the nose tip (Figure 1(c), blue crosses). The regions between the first and second crosses on each side were then selected. The left and right points of the nose, g_L, g_R, were then chosen as the maxima of the angle derivative in these regions,

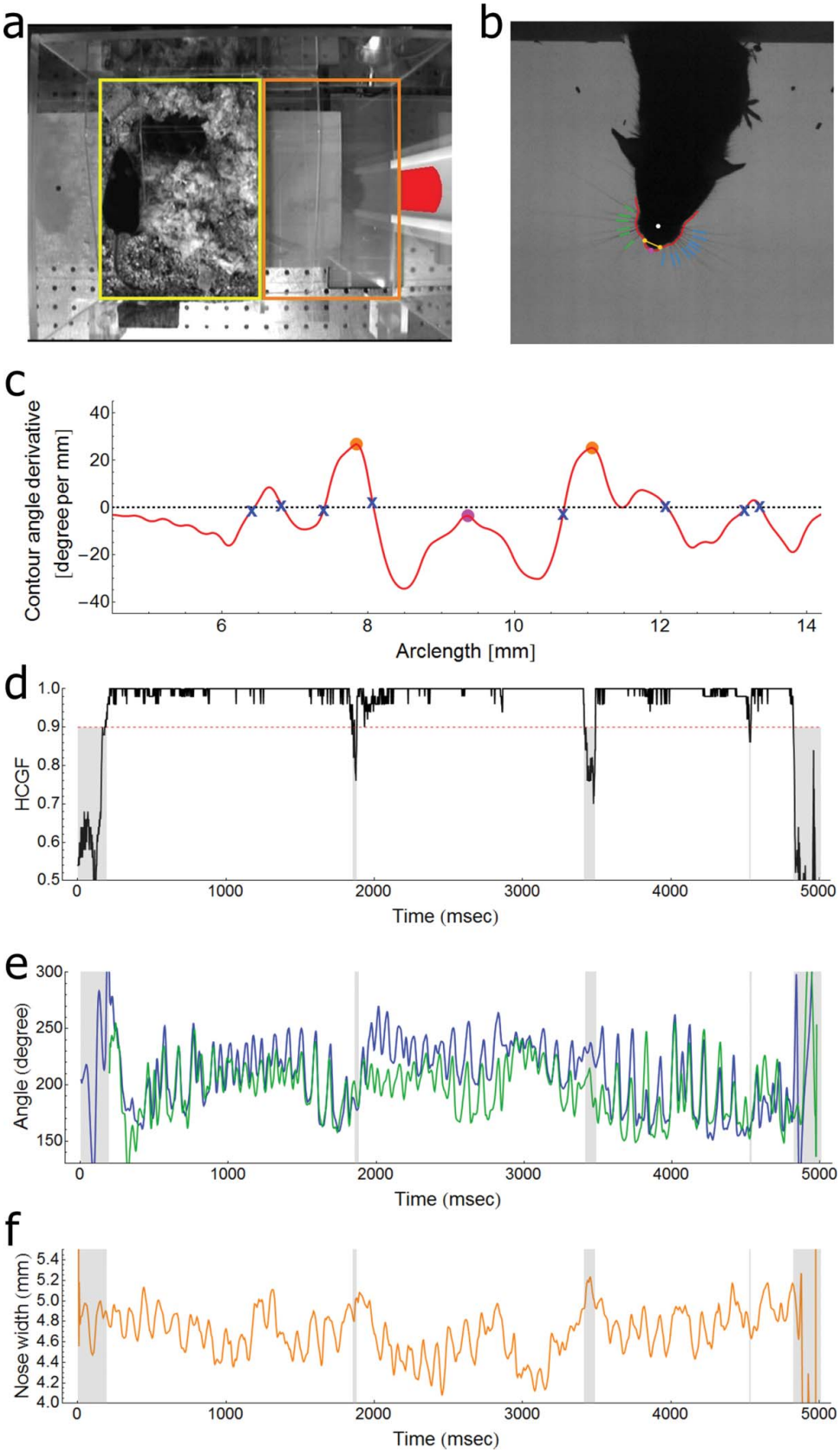

Figure 1. Experimental set-up and measurement of sensory modalities. (a) An image of the home-cage; dam mouse with pups in the nesting chamber (yellow), the transitional chamber (orange) and door area (red). (b) An image from a representative movie (Video S1), where the mouse immerged from the home-cage and performed a round-trip into the novel area. The automatically detected snout contour (red), center of snout (white), nose-tip (magenta), whiskers (left-hand side in blue and right-hand side in green) and the width of the nose (orange) are illustrated upon the image. (c) The contour angle derivative (red), centered on the nose tip (magenta). The frames for which the contour curves, i.e. angle derivative changes sign, are marked by blue-crosses and the zero-line is marked by a dashed black line. The first maxima of change next to the nose tip designate the sides of the nose (orange dots). (d) The head contour goodness-of-fit (HCGF; Perkon et al. 2011) of a representative round-trip. The dashed red line indicates the threshold, above which frames were taken for analysis. Frames below threshold are shaded in light-gray. (e) Whiskers mean angle trace for the left (blue) and right (green) side for the same round-trip as in (d). (f) Nose-width trace for the same round-trip as in (e). Light-gray shaded stripes in (e,f) corresponds to the frames below threshold as presented in (d).

$g_L = \arg\max_{s\in[c_{-2},c_{-1}]} \partial_s\alpha(s)$, $g_R = \arg\max_{s\in[c_{+1},c_{+2}]} \partial_s\alpha(s)$ (Figure 1(b) and 1(c), orange dots). The width of the nose is calculated as the Euclidean distance between these two points. The dynamics of this parameter, i.e. the change of nose-width for each frame, is considered here as a correlate of sniffing (see validations in the Results section).

Nose anatomy

To clarify which of the anatomical structures are responsible for the changes of the nose horizontal diameter, a series of histo-anatomical experiments was performed on 3-week-old C57BL/6 mice because their bones can be cut with a regular microtome. Mice were anesthetized with urethane [25% (w/v), 0.65 mL/100 g body weight, i/p], perfused transcardially with 4% (w/v) paraformaldehyde and 5% (w/v) sucrose in 0.1 M phosphate buffer, pH 7.4. Nasal architecture was visualized in 40 μm thick horizontal, coronal and tangential slices of the snout after staining for cytochrome oxidase activity that was performed according to the method described by Wong-Riley (1979) and modified by Haidarliu and Ahissar (2001). Briefly, the slices were incubated in 0.02% (w/v) of cytochrome c (Sigma-Aldrich, St. Louis, MO), catalase (200 μg/mL) and 0.05% (w/v) diaminobenzidine in 0.1 M phosphate buffer (pH 7.4) at room temperature. The incubation was arrested by adding 0.5 mL of phosphate buffer into each well when the muscles became dark brown. Then the slices were mounted on slides, dried, cover-slipped with Entellan (Merck) and examined and photographed using Nikon Eclipse 50i microscope (Figure 2(a)).

Measurement of air pressure in the nasal cavity

In order to validate that the novel sniffing-detection algorithm correctly captures the sniffing signal, we measured the pressure in the nasal cavity while simultaneously recording video. A hole was drilled into the thickest region of a mouse nasal bone, and a cannula connected to a pressure transducer was inserted through the drilled hole to the nasal cavity (as described in Verhagen et al. 2007 and detailed in Section 2 of the Supplemental data). After full recovery of 1 week, the mouse was free to explore a novel arena that contained odor stimuli (detailed in Section 2 of the Supplemental data). The pressure signal was band-pass filtered between 3 and 25 Hz and down sampled to 500 Hz to match the video sampling rate.

Statistical analysis

Correlations between the nose-width, chest-width and nasal-pressure were tested for statistical significance using a bootstrapping procedure. To generate a null hypothesis, we randomly permuted trial ordering of nose-width, chest-width and nasal-pressure measurements (independently), then computed the pairwise cross-correlation between the randomly permuted data-sets, and averaged over all trials (using Matlab). The procedure was repeated 1000 times to generate a null distribution, from which a p-value was drawn.

Differences between the three exploratory modes, in any measurement, were tested for statistical significance using, unless stated otherwise, one way analysis of variance (ANOVA). The ANOVA tables for all the tests presented in the paper are presented in Section 4 of the Supplemental data. When a significant difference was found, we used Tukey's *post hoc* test in order to localize the significant effect. Whenever the distributions were significantly skewed, we used monotonous transformation to retain normality. For example, for the whisking correlations (Figure 4(f)) and for the sniffing−whisking correlations (Figure 4(g)), we applied 3.1^x transformation, that corrected the skewed distributions (correspondingly $p = 0.72$ and $p = 0.80$ in the Kolmogorov−Smirnov test for normality).

Smoothing

The whisker traces (Figure 1(e)) and sniffing traces (Figure 1(f)) were smoothed with a moving window of 20 msec (10 frames).

Data analysis: pooling the data of the mother and pups

In some of the measures, the absolute values differ between the pups and their mother, for example, in nose-width. However, all mice shared similar variance and relations between the exploratory modes, therefore, in order to be able to pool together all the data for the analysis, we used a mouse-based standardized z-score: $x_{\text{standardized}} = (x - \text{mean}(x))/\text{std}(x)$.

Results

Nose-width is correlated with nasal air-flow

We first explored the anatomical basis of the nose-width signal. In horizontal slices that were cut at the level of the nostrils, the continuity of the nasal cartilaginous capsule was broken by the nostrils (Figure 2(aI)). Such a gap in cartilage continuity makes possible movement of the lateral nasal wall of the nose in the lateral direction that leads to an increase of the horizontal diameter both of the nostrils, as described in rats by Deschênes et al. (2014), and of the rostral part of the nasal vestibule. Increase of the horizontal diameter of the nostrils and of the nasal vestibule can be caused by the contraction of the muscles attached to the lateral wall of the nasal cartilaginous capsule (Figure 2(aII), 2(aIII) and 2(aIV)) that pull the nasal wall laterocaudally. When the muscles relax, the nose restores its initial shape owing to the elastic forces of the nasal cartilage. Given this anatomical basis, we studied the correlation of the nose-width signal with physiological markers of nasal air-flow.

Noticing that breathing is visible in the recorded mouse (see Video S1) we extracted from each frame the width of the chest, approximated by the area of a region of interest across the mouse trunk (Figure 2(b), purple), thus getting a "breathing signal" (Figure 2(c), purple)

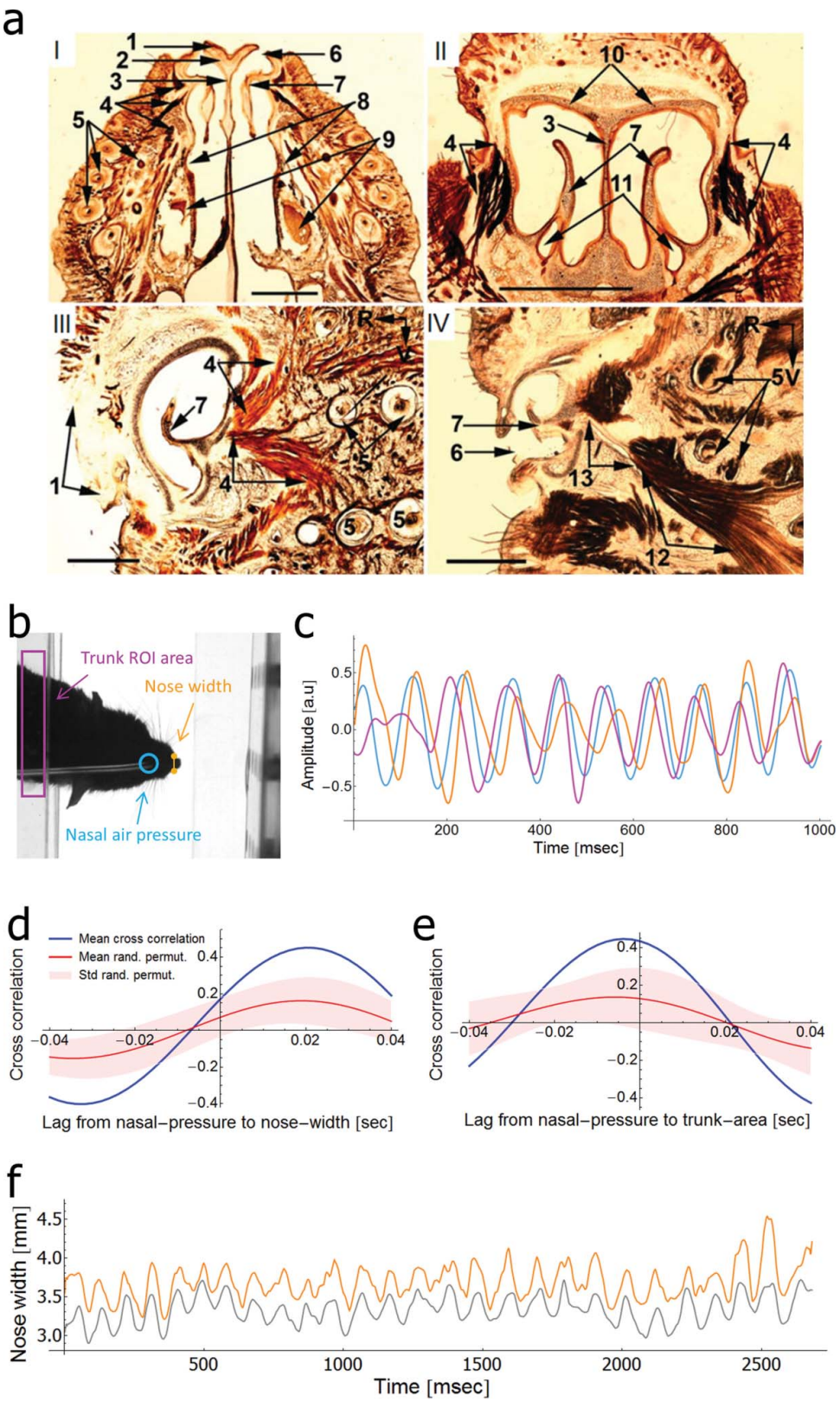

Figure 2. Validation of the sniffing measurement. (a) Histoanatomy of the rostral segment of the mouse nose: (i) horizontal slice of the snout at the level of nostrils, (ii) coronal slice of the snout at the level of nasal vestibule, (iii) superficial tangential slice of the snout and (iv) deep tangential slice of the snout. (1) Rhinarium, (2) lateral ventral process of the septal cartilage, (3) and (4) origins of the muscles attached to the lateral wall of the nasal cartilaginous capsule, (5) vibrissal follicles, (6) nostril, (7) atrioturbinate, (8) premaxilla, (9) incisives, (10) nasal tectum (roof cartilage), (11) nasolacrimal channel, (12) pars maxillaris superficialis of the M. nasolabialis profundus that is attached by a tendon and (13) to the nasal cartilaginous capsule. R: rostral, V: ventral. Scale bars = 1 mm. (b) Independent measurements of air-flow: area of the trunk (magenta), nasal air-pressure via transplanted cannula (light blue) and nose-width (orange). (c) Example of the output signals of the former three methods, color scheme as in (b). (d) Cross correlation between nasal air-pressure and nose-width. (e) Cross correlation between nasal air-pressure and trunk area. (f) Manual (gray) and automatic (orange) scoring of the nose-width.

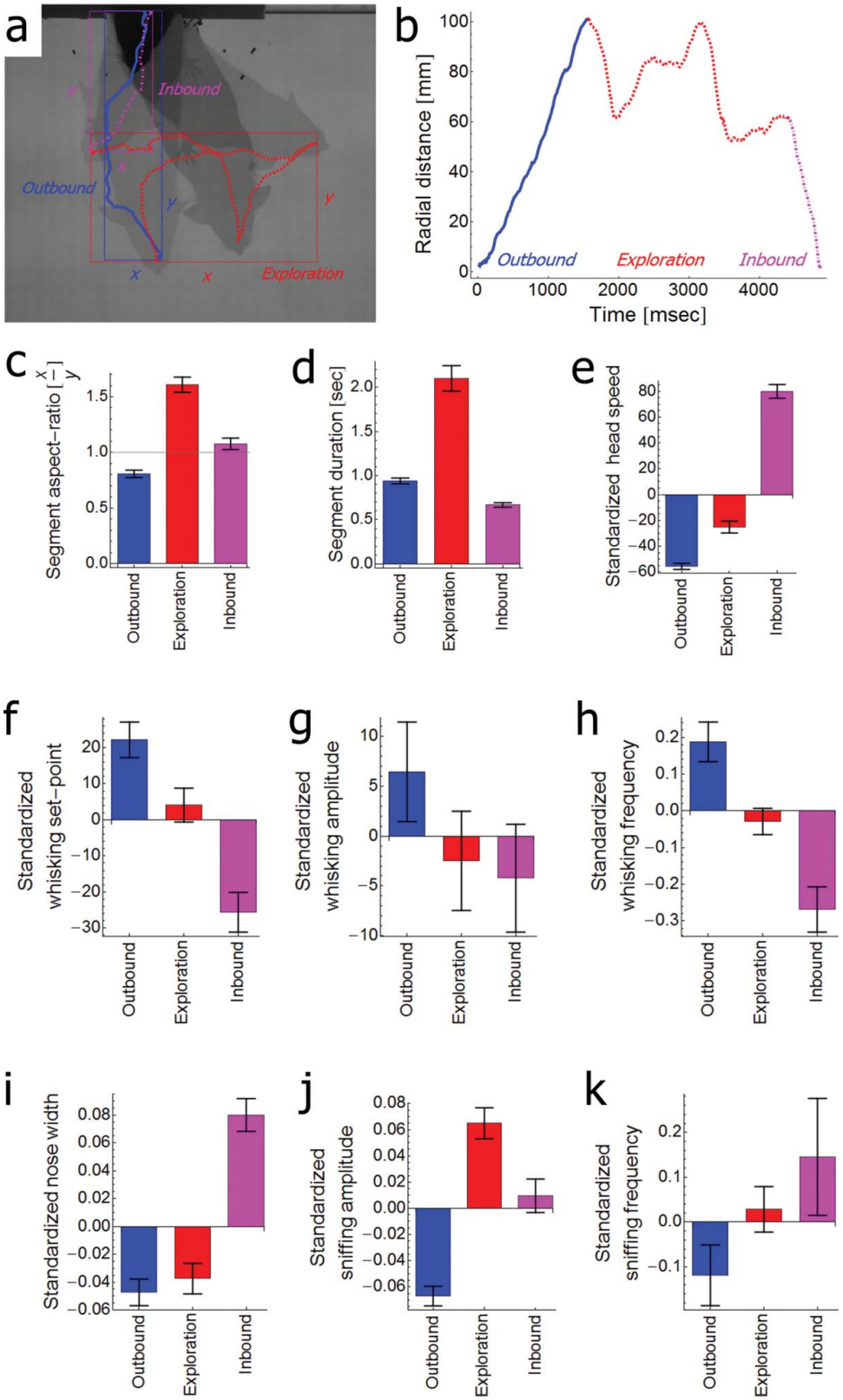

Figure 3. Decomposition of the round-trip trajectory into three exploratory modes and their characteristic measurements. (a) A composite image of several frames from a movie of a mouse performing a single round-trip outside the nest-cage in the exposed area. The trajectory is segmented into Outbound (solid blue), Exploration (dashed red) and Inbound (dot−dashed magenta) modes, confined by their bounding boxes. (b) The color-coded radial distance of the trajectory presented in (a). (c) The aspect ratio (x/y) of the bounding rectangle for all segments of the three exploratory modes. (d) Segment duration. (e) The characteristic highest head speed (quantile 0.95) in each mode. (f−h) Dependence of whisking variables on the exploratory mode: (f) whisking set-point, (g) peak-to-peak amplitude and (h) frequency. (i−k) Dependence of sniffing variables on the exploratory mode: (i) nose-width, (j) peak-to-peak amplitude and (k) frequency. Error bars denote standard error of the mean (SEM). All pair-wise correlations presented in this figure were statistically significant except for: panel (d) (differences were significant only between Exploration and the other two modes); panel (f) (differences were significant only between Outbound and the other two modes); panel (g) (no significant differences were found); panel (i) (differences were significant only between Inbound and the other two modes) and panel (k) (no significant differences were found). All significant differences were highly significant ($p < 0.0001$, ANOVA). Data used in (e−k) was standardized (z-score) as described in the Material and methods section.

where the chest is periodically broadening (inhaling phase) and contracting (exhaling phase). To probe nasal air-flow, we implanted a pressure sensor in the nasal cavity (Figure 2(b), light blue; Section 2 in the Supplemental data). The three signals, nose-width, nasal-pressure and chest-width exhibited a periodic, highly correlated behavior (Figure 2(c)). Correlation strengths and phase relationships are depicted in Figure 2(d) and 2(e). These findings show that nose-widening is concurrent with exhaling and nose-narrowing is concurrent with inhaling.

Finally, we calculated the correlation between the measurements of the nose-width by our automatic algorithm (see Methods section and Figure 1(b) and 1(c)) and by human observers. A 3 sec video (1500 frames) was manually tracked and from each frame the coordinates of maximum curvature on both sides of the nose (orange dots in Figure 1(b)) were extracted. The nose-width was calculated as the Euclidian distance between these points. The correlation between the resulting signal (Figure 2(f), gray line) and the output of the automatic algorithm (Figure 2(f), orange line) was high (Pearson's $r = 0.81$).

Exploration behavior is composed of three modes

Gross analysis of the round-trips into the exposed arena outside the nest-cage revealed three modes (Figure 3(a)): (1) an Outbound portion, where the mouse emerged from the nest-cage and progressed away from the doorway. This mode was defined as the first period after door crossing of the mouse head in which the radial distance from the doorway monotonically increased (Figure 3(b), blue), (2) an Exploration portion, where the mouse typically moved in various directions, defined for every round-trip as the period between Outbound and Inbound (Figure 3(b), red), and (3) an Inbound portion, during which the mouse returned to the nest-cage, defined as the last period during which the radial distance from the doorway monotonically decreased (Figure 3(b), magenta). The aspect ratio of the bounding rectangle differed significantly between the three exploratory modes (Figure 3(c); $p < 0.0001$, ANOVA, Tukey's *post hoc* test shows significant differences between all modes), where Outbound segments score lowest, presenting aspect ratios smaller than 1 (i.e. radially emerging outside in a relatively straight line), and Exploration segments score the highest, aspect ratios larger than 1, reflecting more lateral movements. Furthermore, the segments differed in their duration, with the Exploration segment being the longest (Figure 3(d); $p < 0.0001$, ANOVA). As previously reported (Tchernichovski & Golani 1995), we found that the three modes were significantly different in their peak (quantile 0.95) locomotion speed ($p < 0.0001$, ANOVA) where in the Inbound portion mice reached highest speeds and in Outbound portion − lowest speeds (Figure 3(e)).

Exploratory modes have different whisking and sniffing characteristics

For both whisking and sniffing, we analyzed the following variables: the set-point (the mean), the amplitude and the central frequency within a 500 msec sequence (Table 1).

Whisking

Whisking set-point significantly decreased from Outbound, via Exploration to Inbound ($p < 0.0001$, ANOVA; Figure 3(f)). Whisking amplitude (Figure 3(g)) showed no significant differences for all three modes ($p = 0.28$, ANOVA). Whisking frequency significantly decreased from Outbound, via Exploration to Inbound ($p < 0.0001$, ANOVA; Figure 3(h)).

Sniffing

Nose-width set-point (mean width) was similar during Outbound and Exploration and increased during the Inbound mode ($p < 0.0001$, ANOVA; Figure 3(i)). Sniffing amplitude increased from Outbound to Exploration and decreased again during the Inbound mode ($p < 0.0001$, ANOVA; Figure 3(j)). Sniffing frequency showed no significant differences between locomotion modes ($p = 0.09$, ANOVA; Figure 3(k)).

In summary, during the Outbound mode, mice typically pulled their whiskers forward and narrowed their noses while whisking at high frequencies and sniffing at low amplitudes. During Exploration, they typically balanced their whiskers' set-points and maintained narrow noses while increasing sniffing dynamic range (i.e.

Table 1. Whisking and sniffing characteristics.

Measure name	Mean	SD	Trimmed range	Units
Whiskers left set-point angle	217.8	46.6	∼(168.4−257.2)	deg.
Whiskers right set-point angle	218.2	28.6	∼(179.7−245.1)	deg.
Nose width	4.6	0.3	∼(4.2−5.2)	mm
Whisking left amplitude	83.1	29.4	∼(43.4−135.0)	deg.
Whisking right amplitude	81.7	46.5	∼(48.1−117.0)	deg.
Sniffing amplitude	1.1	0.4	∼(0.6−1.7)	mm
Whisking left (frequency)	12.9	4.0	∼(8.3−20.0)	Hz
Whisking right (frequency)	12.7	4.0	∼(8.3−20.0)	Hz
Sniffing (frequency)	10.4	2.6	∼(8.3−16.7)	Hz
Head speed	125.7	60.8	∼(49.7−240.2)	mm/s

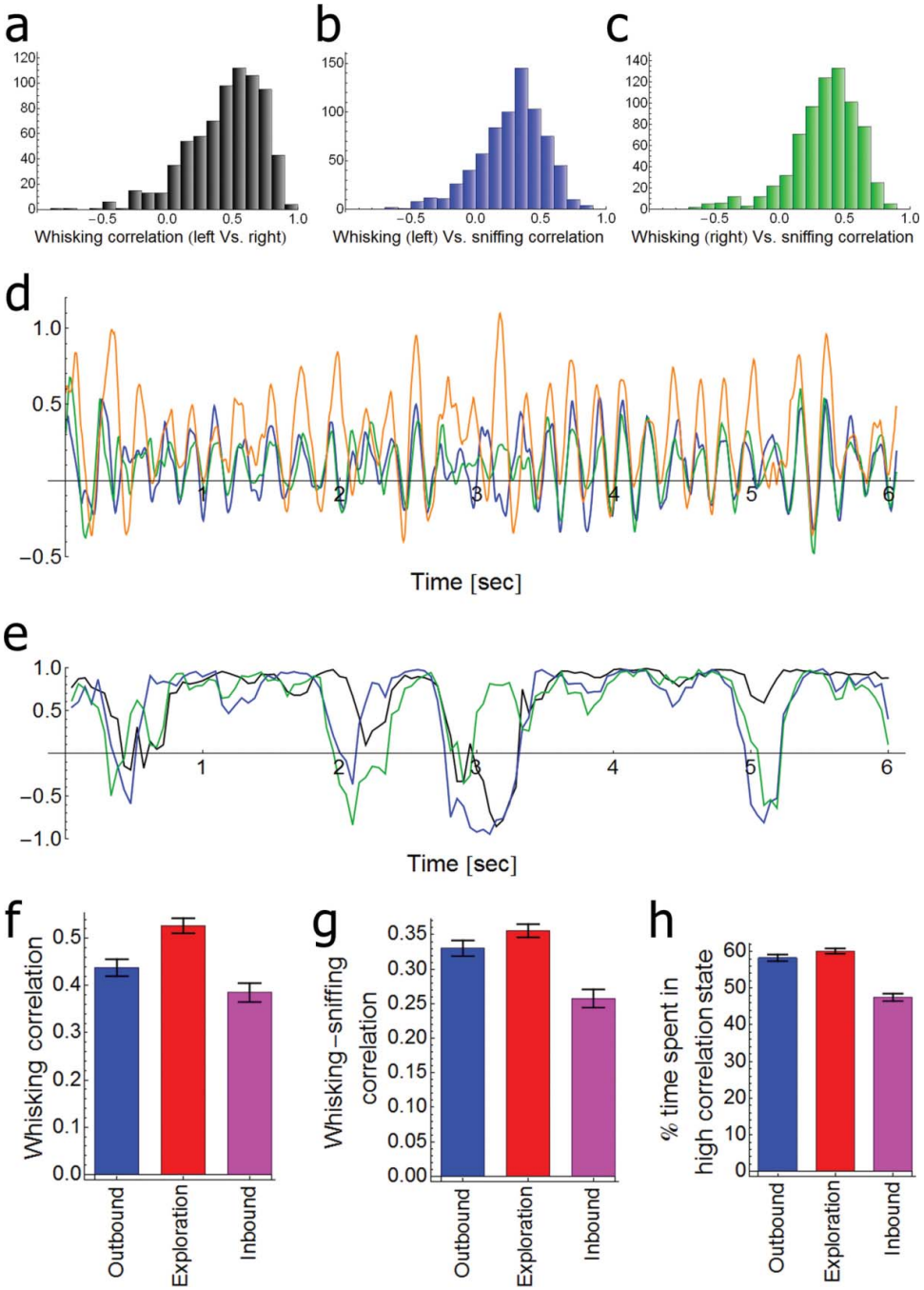

Figure 4. Whisking and sniffing correlations. (a)–(c) Distribution of correlation coefficients between right and left whisking angles (black), sniffing and left whisking angles (blue) and sniffing and right whisking angles (green). (d) An example of whisking (left – blue, right – green) and sniffing (orange) signals. (e) Moving window correlation time series for the signals presented in (d); left vs. right side whisking (black), left whisking – sniffing (blue) and right whisking – sniffing (green). (f) Whisking correlation dependence on the exploratory mode; correlation during Exploration was significantly higher. (g) Whisking – sniffing correlation dependence on the exploratory mode; correlation during Inbound was significantly lower. (h) The percentage of time spent in the high correlation ($r > 0.5$) state. Percentage during Inbound was significantly lower. Error bars denote SEM. All significant differences were highly significant ($p < 0.0001$, ANOVA).

amplitude). During the Inbound mode, they typically retracted their whiskers and widened their noses, while whisking at a low frequency.

Whisking and sniffing correlation

We analyzed the correlation between left and right whisking angles (Figure 4(a)). As can be seen, the distribution of correlation coefficients is strongly skewed towards strong positive correlations, though lower positive and negative correlations also existed. No strong negative correlations were found in this study.

Correlations between whisking and sniffing were in general weaker than inter-whisker correlations, although exhibiting a similar variability (Figure 4(b) and 4(c)). On average, inter-whisker correlations showed significant increase during the Exploration mode ($p < 0.0001$, ANOVA; Figure 4(f)) and inter-modal correlations

Table 2. Percentage of time at high correlation ($r > 0.5$).

Modality: exploratory mode:	Left−right	Sniff-left	Sniff-right
Outbound	62.7 ± 24	53.9 ± 24	58.9 ± 24
Exploration	66.8 ± 19	55.3 ± 17	58.2 ± 17
Inbound	56.0 ± 27	43.2 ± 25	43.3 ± 27

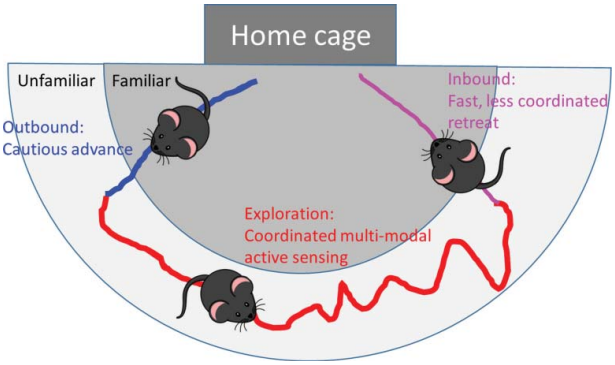

Figure 5. An illustration of our interpretation of the whisking-sniffing parameters and correlation for the three exploratory modes. Outbound (blue): cautious mode with low head speed and protracted whiskers, Exploration (red): whisking and whisker-sniffing coordinated exploration, and Inbound (magenta): high head speed retreat with less coordinated sensing.

decreased during the Inbound mode ($p < 0.0001$, ANOVA; Figure 4(g)). Importantly, however, a close examination of individual trials revealed that the sniffing−whisking correlations and inter-whisker correlations fluctuated together, switching between long periods ("states") of high correlations ($r > 0.5$) and shorter periods of varying correlations (Figure 4(d) and 4(e); Section 3 in the Supplemental data). Interestingly, both intra-modal and inter-modal correlations generally changed in general together. Yet, switching from the correlated to uncorrelated states was often not fully synchronized (see examples of uncorrelated signals in Figure 4(d) and 4(e) and Section 3 in the Supplemental data). These correlations of active sensing dynamics were significantly affected by the exploratory mode. The percentage of time spent in the high correlation state was significantly lower during the Inbound mode (Figure 4(h); Table 2). The results of a two-way ANOVA show both mode effect where during the Inbound mode the correlations were significantly lower ($p < 0.0001$), and modality effect where the correlations between left and right whisking were significantly higher ($p < 0.0001$), with no interaction ($p = 0.09$; Table 2).

Discussion

In this study, we examined a complex agent-environment system, wherein mice explored a novel arena. We analyzed, both separately and jointly, two major sensory modalities in mice − whisking and sniffing. We implemented an ethological approach using a free exploration paradigm, developed an innovative sniffing detection algorithm based on image processing that for the first time allowed the collection of simultaneous bi-modal data of active sensing behavior of freely ranging animals based solely on non-invasive techniques.

We categorized the interactions of our mice with their environment to three major categories (Figures 3(a) and 5): an Outbound segment, characterized by a low head-speed approach to a novel place; an Exploration segment, characterized by long duration and lateral movements within a novel area; and an Inbound segment, characterized by high-speed returns to the home-cage. We found that mice exhibit a highly coordinated multimodal active sensing in the Outbound and Exploration segments. In the Exploration segment, left−right whisking and whisking−sniffing correlation were highest, whereas in the Inbound mode, whisking and sniffing were less powerful and also less correlated.

During the Outbound segment, head speed was lowest, while the whisker set-point was highest, consistent with previous results (Arkley et al. 2014). This may indicate a cautious behavior, aiming at reducing the danger of hitting unexpected objects with the nose.

Whisking−sniffing coordination was also studied in Ranade et al. (2013), where phase-locked whisking and sniffing was found during exploration bouts. In Cao et al. (2012), a variability in sniffing−whisking correlation was found in head-fixed mice, that depended on the whisking frequency. Our findings suggest that indeed there is large variability in sniffing−whisking correlation also in freely moving mice and that this depends on context or exploratory mode.

The neural mechanism behind this whisking−sniffing correlation is yet unknown, although the brainstem has been suggested to play an important role (Moore et al. 2014). Given the variability of correlation we found, neural control of whisking and sniffing may be realized at multiple levels (Moore et al. 2013). Similar conclusions were reached in a study that measured whisking and sniffing in head-fixed mice (Cao et al. 2012) as well as in a study that examined whisking and sniffing during an open-field reward foraging behavior and found different modes of phase locking (Ranade et al. 2013).

The high variability of the correlation between whisking and sniffing that was revealed in our study can be also explained by the involvement of different groups of facial muscles in the functioning of both vibrissal and olfactory motor plants that were described in rats and mice (Hill et al. 2008; Haidarliu et al. 2015). Three subunits of the M. nasolabialis profundus (Partes maxillares superficialis et profunda, and Pars interna profunda) have their origins on the outer wall of the nasal cartilage that surrounds nasal atrium, and insert into the deep fibrous mat of the mystacial pad. Contraction of these muscles has a dual effect: it pulls the wall of the lateral nasal cartilage outward, thus dilating the nares and nasal vestibule, and produces a retraction of the vibrissae by pulling the deep fibrous mat rostrally, together with the proximal ends of the vibrissal follicles (Deschênes et al. 2014). The nasal vestibule acquires its initial shape when the muscles relax. However, during

exploratory whisking, vibrissa protracting parts of the M. nasolabialis profundus that originate similarly from the nasal cartilage, also can be activated causing dominating vibrissa protraction. Variation of simultaneously contracted facial muscles can explain the variability of correlation observed between whisking and sniffing.

The complex dynamics of exploration in the natural settings studied here involve a freely moving agent with several sensors with which it can learn about its environment. We have shown, using the novel non-invasive tools we have developed, that there is an intricate interplay between the exploratory mode of the mice, and the patterns and coordination of their active multi-modal sensing. This suggests an underlying complex neural network that regulates information intake from the environment on several time scales, namely, exploration segments controlled by locomotion and, active sensing controlled by whiskers and snout. In principle, such a complex network could be implemented as an integration of individual networks, each processing the output of an individual modality (Angelaki et al. 2009). However, the tight motor correlations presented here, and their modulation by the exploratory mode, strongly suggest that the modalities are interacting at multiple levels. Optimal Bayesian integration of multi-modal sensory information has been suggested before (Hillis et al. 2002; Körding & Wolpert 2004), for proprioception and vision (van Beers et al. 1999), texture and motion (Jacobs 1999) and vision and haptics (Ernst & Banks 2002). However, these open-loop perceptual-based studies did not explore active-sensing, whereas the results presented here suggest closed-loop control (Deutsch et al. 2012; Saig et al. 2012), allowing sensory−motor coordination at several levels of resolution, very much like individual pathways interact within each modality (Ahissar & Kleinfeld 2003). The coordination of such a complex multiple-level multiple-modality system can be done via a novelty-based management architecture (Gordon et al. 2014); the expectation-based tuning of the sensors and their coordination observed in this study supports this possibility.

To conclude, we have developed a non-invasive tool to simultaneously record whisking and sniffing in freely moving and exploring mice. We have shown that the correlation between these modalities is variable and depends on the context with which they are used, e.g. exploration or return to a home cage. We propose that these tools can be used in a wide variety of experimental designs to increase our understanding of the behavioral as well as underlying neuronal mechanisms of these important active sensory modalities.

Acknowledgements

We thank Inbar Saraf-Sinik for her help in validating the nose tracking technique and Aharon Weissbrod for the help in establishing the nasal air pressure apparatus. This research was supported by the Israel Science Foundation [grant no. 1127/14]; the Minerva Foundation funded by the Federal German Ministry for Education and Research, the United States-Israel Binational Science Foundation (BSF) [grant 201143] and the NSF-BSF Brain Research EAGER program [grant number 2014906]. Ehud Ahissar incumbent of the Helen Diller Family Professorial Chair of Neurobiology. Ehud Fonio incumbent of the Tom Beck Research Fellow Chair in Physics of Complex Systems.

Disclosure statement

No potential conflict of interest was reported by the authors.

Funding

This research was supported by the Israel Science Foundation [grant number 1127/14]; the Minerva Foundation funded by the Federal German Ministry for Education and Research, the United States-Israel Binational Science Foundation (BSF) [grant number 201143]; the NSF-BSF Brain Research EAGER program [grant number 2014906].

Supplemental data

Supplemental data for this article can be accessed here.

References

Ahissar E, Kleinfeld D. 2003. Closed-loop neuronal computations: focus on vibrissa somatosensation in rat. Cereb Cortex. 13:53−62.

Angelaki DE, Gu Y, DeAngelis GC. 2009. Multisensory integration: psychophysics, neurophysiology, and computation. Curr Opin Neurobiol. 19:452−458.

Arkley K, Grant RA, Mitchinson B, Prescott TJ. 2014. Strategy change in vibrissal active sensing during rat locomotion. Curr Biol. 24:1507−1512.

Berg RW, Kleinfeld D. 2003. Rhythmic whisking by rat: retraction as well as protraction of the vibrissae is under active muscular control. J Neurophysiol. 89:104−117.

Cao Y, Roy S, Sachdev RN, Heck DH. 2012. Dynamic correlation between whisking and breathing rhythms in mice. J Neurosci. 32:1653−1659.

Deschênes M, Haidarliu S, Demers M, Moore J, Kleinfeld D, Ahissar E. 2014. Muscles involved in naris dilation and nose motion in rat. Anat Rec. 298:546−553.

Deschênes M, Moore J, Kleinfeld D. 2012. Sniffing and whisking in rodents. Curr Opin Neurobiol. 22:243−250.

Deutsch D., Pietr M, Knutsen PM, Ahissar E, Schneidman E. 2012. Fast feedback in active sensing: touch-induced changes to whisker-object interaction. PLOS One 7:e44272.

Eilam D, Golani I. 1989. Home base behavior of rats *Rattus norvegicus* exploring a novel environment. Behav Brain Res. 34:199−211.

Ernst MO, Banks MS. 2002. Humans integrate visual and haptic information in a statistically optimal fashion. Nature 415:429−433.

Fonio E, Benjamini Y, Golani I. 2009. Freedom of movement and the stability of its unfolding in free exploration of mice. Proc Natl Acad Sci USA. Dec;106:21335−21340. Epub 2009 Nov 26.

Gao P, Bermejo R, Zeigler HP. 2001. Whisker deafferentation and rodent whisking patterns: behavioral evidence for a central pattern generator. J Neurosci. 21:5374−5380.

Golani I, Benjamini Y, Eilam D. 1993. Stopping behavior: constraints on exploration in rats *Rattus norvegicus*. Behav Brain Res. 53:21−33.

Gordon G, Fonio E, Ahissar E. 2014. Emergent exploration via novelty management. J Neurosci. 34:12646−12661.

Grant RA, Mitchinson B, Fox CW, Prescott TJ. 2009. Active touch sensing in the rat: anticipatory and regulatory control of whisker movements during surface exploration. J Neurophysiol. Feb;101:862−874. Epub 2008 Nov 28.

Haidarliu S, Ahissar E. 2001. Size gradients of barreloids in the rat thalamus. J Comp Neurol. 429:372−387.

Haidarliu S, Kleinfeld D, Deschênes M, Ahissar E. 2015. The musculature that drives active touch by vibrissae and nose in mice. Anat Rec. 298:1347−1358.

Hill DN, Bermejo R, Zeigler HP, Kleinfeld D. 2008. Biomechanics of the vibrissa motor plant in rat: Rhythmic whisking consists of triphasic neuromuscular activity. J Neurosci. 2008;28:3438−3455.

Hillis JM, Ernst MO, Banks MS, Landy MS. 2002. Combining sensory information: mandatory fusion within, but not between, senses. Science 298:1627−1630.

Jacobs RA. 1999. Optimal integration of texture and motion cues to depth. Vis Res. 39:3621−3629.

Kepecs A, Uchida N, Mainen ZF. 2007. Rapid and precise control of sniffing during olfactory discrimination in rats. J Neurophysiol. 98:205−213.

Knutsen PM, Pietr M, Ahissar E. 2006. Haptic object localization in the vibrissal system: behavior and performance. J Neurosci. Aug;26:8451−8464. Epub 2006 Aug 18.

Koelewijn T, Bronkhorst A, Theeuwes J. 2010. Attention and the multiple stages of multisensory integration: a review of audiovisual studies. Acta psychologica. 134:372−384.

Körding KP, Wolpert DM. 2004. Bayesian integration in sensorimotor learning. Nature 427:244−247.

Macrides F, Eichenbaum HB, Forbes WB. 1982. Temporal relationship between sniffing and the limbic rhythm during odor discrimination reversal learning. J Neurosci. 2:1705−1717.

Mitchinson B, Martin CJ, Grant RA, Prescott TJ. 2007. Feedback control in active sensing: rat exploratory whisking is modulated by environmental contact. Proc Biol Sci. Apr.274:1035−1041. Epub 2007 Mar 03.

Moore JD, Deschênes M, Furuta T, Huber D, Smear MC, Demers M, Kleinfeld D. 2013. Hierarchy of orofacial rhythms revealed through whisking and breathing. Nature.497:205−210.

Moore JD, Kleinfeld D, Wang F. 2014. How the brainstem controls orofacial behaviors comprised of rhythmic actions. Trends Neurosci. 37:370−380.

Perkon I, Kosir A, Itskov PM, Tasic JF, Diamond ME. 2011. Unsupervised quantification of whisking and head movement in freely moving rodents. J Neurophysiol. 105:1950−1962.

Ranade S, Hangya B, Kepecs A. 2013. Multiple modes of phase locking between sniffing and whisking during active exploration. J Neurosci. 33:8250−8256.

Saig A, Gordon G, Assa E, Arieli A, Ahissar E. 2012. Motor-sensory confluence in tactile perception. J Neurosci. 32:14022−14032.

Semba K, Komisaruk BR. 1984. Neural substrates of two different rhythmical vibrissal movements in the rat. Neuroscience. Jul;12:761−774. Epub 1984 Jul 01.

Tchernichovski O, Benjamini Y, Golani I. 1998. The dynamics of long-term exploration in the rat. Part I. A phase-plane analysis of the relationship between location and velocity. Biol Cybern. Jun;78:423−432. Epub 1998 Aug 26.

Tchernichovski O, Golani I. 1995. A phase plane representation of rat exploratory behavior. J Neurosci Methods. 62:21−27.

Uchida N, Mainen ZF. 2003. Speed and accuracy of olfactory discrimination in the rat. Nat Neurosci. 6:1224−1229.

Von Uexküll, J. (1957). A stroll through the worlds of animals and men: A picture book of invisible worlds. In CH Schiller, editor. Instinctive behavior: The development of a modern concept. New York: International Universities Press; p. 5−80. (Original work published 1934).

van Beers RJ, Sittig AC, Gon JJ. 1999. Integration of proprioceptive and visual position-information: an experimentally supported model. J Neurophysiol. 81:1355−1364.

Verhagen JV, Wesson DW, Netoff TI, White JA, Wachowiak M. 2007. Sniffing controls an adaptive filter of sensory input to the olfactory bulb. Nat Neurosci. 10:631−639.

Vincent, S. 1912. The function of the vibrissae in the behavior of the white rat. In: Behavior monographs, Vol. 1, Series 5. Chicago: University of Chicago; p. 1−81.

Welker WI. 1964. Analysis of sniffing of the albino rat. Behaviour. 22:223−244.

Wesson DW, Carey RM, Verhagen JV, Wachowiak M. 2008. Rapid encoding and perception of novel odors in the rat. PLOS Biol. 6:e82.

Wong-Riley MTT. 1979. Changes in the visual system of monocularly sutured or enucleated cats demonstrable with cytochrome oxidase histochemistry. Brain Res. 171:11−28.

Zuo Y, Perkon I, Diamond ME. 2011. Whisking and whisker kinematics during a texture classification task. Phil. Trans. R. Soc. B. 366:3058−3069.